FEAST

The Far and Extreme UV Astrophysical Spectral Telescope

M. Berretti, A. Binios, V. Foss, J. Gillmayr, J. Jacobs, V. Kutnohorsky, F. af Malmborg, D. Manzini, J. Matias, F. Oggionni, A. Pedersen, L. Sisovas, and M. Viviano[*]

ABSTRACT

The Far and Extreme UV Astrophysical Spectral Telescope (FEAST) aims to further our understanding of the formation of high-energy events in Sun-like stars and the extreme ultraviolet (EUV) radiation incident on exoplanet atmospheres. An innovative mission concept, it will provide our first observations of the EUV environments of other stars within our local galactic bubble. As we seek to further our understanding of our place within our solar system and beyond, this mission will expand our limited knowledge of stellar EUV environments and their long- and short-term variability. With a temporal and spectral resolution capable of resolving the coronal dimming caused by coronal mass ejections (CMEs) FEAST will provide the first observations and measurements of these energetic transient events on stars other than our Sun, giving crucial insight into their relation to stellar flares and improve models for their formation. FEAST will also provide an extential investigation of the EUV radiation emitted by stars hosting exoplanets, giving key insights into models of exoplanet atmosphere evolution.

Using a extreme UV and far UV (EUV/FUV) modified Hettrick-Boyer telescope combined with nested parabolic and hyperbolic grazing incidence mirrors, FEAST will measure incident EUV and FUV radiation with a wavelength resolution of 1 Å and 0.5 Å, respectively. The mission will be deployed to the Lagrangian 2 point (L_2) behind Earth to avoid spectral contamination from Earth's hydrogen-rich geocorona.

Key words. extreme ultraviolet – far ultraviolet – coronal mass ejection – flare – exoplanet atmosphere – space mission – telescope

1. Introduction

While most of the electromagnetic spectrum has been thoroughly observed, the extreme ultraviolet (EUV) waveband remains mostly unknown to this day. The lack of observations is due to the intrinsic physical properties of the interstellar medium, which readily absorbs most of the wavelengths lying in this range. The limited amounts of EUV radiation that reaches our close-Earth environment holds the key to answer important and fundamental questions in both stellar dynamics and exoplanetary science. There is an increasing body of evidence that this elusive wavelength range can help us understand the very nature of high-energy transient events such as flares and coronal mass ejections (CMEs). (Moschou et al. 2019). While we have a rough understanding of the driving and formation of CMEs, we have no information on how different stellar parameter affect their dynamic and frequency. Similarly the EUV radiation produced by stellar-like stars plays a fundamental role for the fate of neighboring exoplanets: in particular intense radiation in this energy ranges is the most important driver of atmospheric evaporation (Cecchi-Pestellini et al. 2009). In this regard, studying exoplanet host stars in the EUV would allow us to further understand the timescales and driving processes for atmospheric loss. This will ultimately help us understand conditions for exoplanet habitability and aid in the search for life within our galactic neighbourhood.

In this report, we present a proposal for a satellite EUV telescope to answer these very questions. The report lies out the science case in detail, the measurement requirements and constraints on the payload, the spacecraft design and the mission design.

2. Science

The EUV flux incident on Earth's atmosphere has been shown to be the primary driver of heating in the upper thermosphere (Lammer et al. 2003). EUV photons $(100-1000)$ Å are absorbed by neutral species, producing ionisation, and liberating energetic electrons that can obtain much higher altitudes than the ions from which they originated. This charge separation causes the formation of an ambipolar electric field which leads to ion outflow and mass loss from the upper atmosphere (Ganguli 1996).

While there is an average steady-state EUV flux from our Sun that correlates to the black-body emission spectrum there are also high-energy, impulsive, transient events known as coronal mass ejections (CMEs) which provide additional, concentrated pulses of energetic plasma. These events produce geomagnetic storms on Earth that are characterized by a change in the ring current, increased D and E region conductivity, and thermospheric heating and expansion. These impulsive events can disrupt power grids, interrupt space-borne communication, and lead to increased drag on low-Earth orbiting spacecraft. Despite their drastic impact on our technology, these events and the dynamics surrounding their formation are not well understood. CMEs have been shown to have a high correlation with other impulsive

---

[*] Summer School Alpbach (e-mail: `FEAST.mission@gmail.com`) – with help from C. Götz, L. Fossati, and G. de Marco
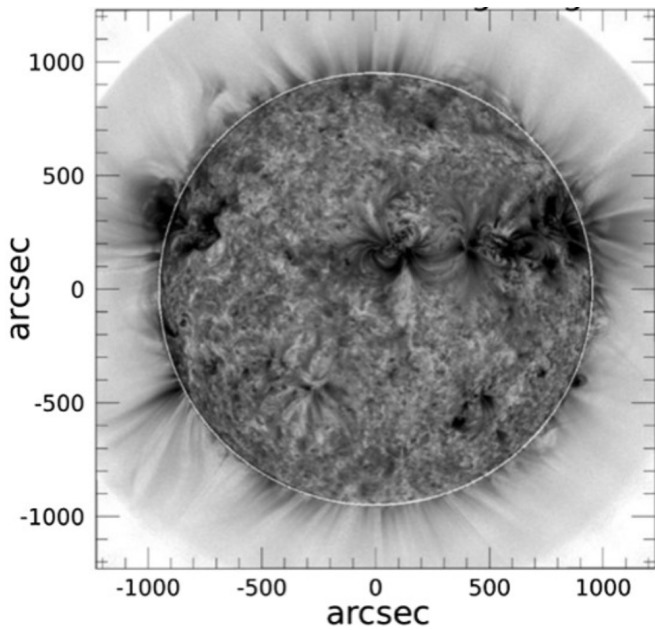
Fig. 2.1. An EUV image of the coronal solar disk displaying multiple regions of dimming associated with CME activity (France et al. 2022).

events known as solar flares, in which a broad electromagnetic impulse is released, often followed by a CME.

We can observe CMEs and flares on our Sun with coronagraphs, EUV imaging, and in-situ measurements. A flare presents as a brief (minutes) increase in intensity across the entire electromagnetic spectrum, while CMEs present as a void in EUV images as seen in Figure 2. Recent studies(Mason et al. 2014; Cheng and Qiu 2016) have demonstrated that these emissions can be more precisely measured through the use of a disk-integrated EUV spectrum. CMEs are highly correlated with a dimming of certain EUV spectral emission lines (e.g., 171 Å) that correspond to the mass loss in the corona. By comparing the relative intensity of 'dimming' and 'non-dimming' lines as a function of time, we can see the temporal evolution of these transient features. Furthermore, the features of the dimming such as the depth and slope can give an insight into the mass and propagation of the ejected plasma, respectively (Veronig et al. 2019; France et al. 2022).

2.1. Scientific Questions

Studying the EUV and FUV of solar-mass stars will contribute to answer the following scientific primary and secondary questions:

Q1: How do stellar properties affect the formation of energetic transient events?
· How are stellar properties such as mass and activity coupled to not only CME formation but also total EUV flux? How does this relationship evolve over long timescales?
· What is the relationship between EUV and FUV variability in solar-mass stars?
Q2: What is the EUV radiation environment experienced by exoplanets orbiting nearby stars?
· How do CMEs affect planetary atmospheres?

2.2. Scientific requirement

In order to answer the first scientific questions, the following required criteria must be established and fulfilled.

S1: The mission shall allow to observe 25 Sun-like stars and detect potential coronal mass ejections.
S2: The mission shall allow to measure coronal dimming, including the onset and decay time.
S3: The mission shall allow to observe at least 10 CMEs in each of the 25 stars.
S4: The mission shall allow to observe 25 Sun-like stars and detect potential stellar flares.
S5: The mission shall allow to measure stellar flares, including onset and decay time.

That the second question can be answered by accomplishing the following requirement.

S6: The mission shall allow measuring the integrated intensity in the EUV and FUV range for 500 stars.
S7: The mission shall allow to measure short-term variability in the EUV range for 500 stars.
S8: The mission shall allow to observe 500 stars for 10 hours.

2.3. Measurement requirements

Different requirements were defined for EUV and FUV measurements.

M1: The EUV instrument shall be able to measure intensity in the wavelength range $(150 - 700)$ Å.
M2: The EUV instrument shall have a spectral resolution of 0.5 Å.
M3: The EUV instrument shall have a signal-to-noise ratio of 100 at a wavelength of 171 Å and 284 Å for an integration time of 10 min.
M4: The FUV instrument shall be able to measure intensity in the wavelength range $(1300 - 1656)$ Å.
M5: The FUV instrument shall have a spectral resolution of 0.2 Å.
M6: The FUV instrument shall have a signal-to-noise ratio of 100 at a wavelength of 1321 Å and 1445 Å for an integration time of 1 min.
M7: The instrument shall have a field of view of 2′.
M8: The instrument shall have a temporal resolution < 1 min.

3. Mission

Mission Statement:

To further our understanding of the formation of high-energy events in Sun-like stars and the EUV radiation incident on exoplanet atmospheres.

As our understanding of the Universe in which we live develops, so has our desire to understand our place within the vast cosmos. Despite our increasing knowledge of EUV solar processes, we are limited by the fact that we have only one point of reference, our Sun.

The study of other stellar atmospheres may help us to understand these complicated dynamics, and whether stellar properties such as mass and rotation rate play a role. Flares, which present as an impulse across the entire electromagnetic spectrum, have been measured on many other stars. The same cannot be said for CMEs or the EUV environment, though this is largely due to a physical complication presented by the interstellar medium (ISM). Comprised of primarily helium and hydrogen, the ISM readily absorbs EUV radiation from distant stars, inhibiting our ability to measure them (Rumph et al. 1994). All hope is not lost though, as these dynamics are less pronounced within our

local bubble, about 90 pc in diameter, which contains over 500 potential stellar targets (Lehner et al. 2003).

By observing these stars in EUV, we can infer how stellar properties such as mass, age, and rotation rate impact energetic transient events (CMEs and flares) and how their correlation varies as a function of the same parameters. By looking at how the correlation between these parameters varies in other stellar environments, it may help us increase our understanding of the physics governing their formation.

Understanding different stellar EUV environments will fill in an important observational gap that can be used as an input in atmospheric models. Stellar winds play an important role in the atmospheric escape, and CMEs are thought to be the dominant source of long-term instability in planetary atmospheres. Similarly, the atmospheres of planets experiencing frequent flares may never achieve a steady state if the timescales for atmospheric recovery are shorter than the flare frequency.

Only one space mission has previously examined the EUV spectrum of stars other than our own. The Extreme-Ultraviolet Explorer (EUVE) launched in 1992 was a survey mission by NASA designed to carry out a full-sky survey searching for EUV sources as well as a few focused observations (Bowyer 1991). The results from this mission provide a catalogue of potential stellar EUV targets, but the EUVE mission did not have enough resolution to study stellar dynamics such as CME occurrence or flares.

To address these gaps in our scientific understanding we propose a new space mission called the Far Extreme UV Astrophysical Spectral Telescope (FEAST). Using a state-of-the-art EUV telescope FEAST will measure in two distinct regimes: (1) FEAST will take long-term (one week) measurements of the nearest Sun-like stars ($\sim$ 25), resolving CME and flare activity to understand the connection between stellar properties and energetic transient events. (2) FEAST will take short snapshots (10 hours) of the entire catalogue of 508 available stars to obtain their overall EUV spectra. We will revisit each star at least 4 times during the mission to understand the variability of this emission. Launched into orbit around L_2, it will be able to resolve the EUV features of our stellar neighbours with unprecedented precision.

3.1. Orbit

The launch phase (phase E1) will last for approximately 40 minutes (Lagier et al. 2021). After that, the Vinci upper stage will perform a burn to place the spacecraft in a highly elliptical orbit with its apogee in the vicinity of L_2 ($\Delta V = 2.5 \text{ kms}^{-1}$). Following the burn, spacecraft separation and subsequent automatic solar panel deployment will occur. The first telemetry data will be received as soon as a few hours after launch when the spacecraft will be in the visibility window of the New Norcia ground station. Critical systems checkups will be commanded and health monitoring data will be periodically sent to Earth by the spacecraft. The transfer trajectory will last for approximately 28 days; during the transfer trajectory, depending on the launcher's injection accuracy, a correction manoeuvre might be performed with the onboard propulsion system. Finally, an orbit insertion manoeuvre will be commanded to enter a Halo orbit ($\Delta V = 40 \text{ ms}^{-1}$). Once the operational orbit is reached, an instrument commissioning phase will begin, lasting for approximately four months. After approx. five months from launch, science operations will be enabled. The nominal mission lifetime (phase E2) is five years, with two years of possible mission extension (phase E3). Orbital correction manoeuvres will be per-

formed once per orbit, together with reaction wheel offloading, accounting for a Delta V of $\Delta V = 6 \text{ ms}^{-1}$ per year. After the end of science operations, an end-of-life manoeuvre will insert the spacecraft into a heliocentric orbit (phase F). Finally, six months from such manoeuvre, a final burn will be performed to minimize the chance of a collision between the spacecraft and the Earth. The spacecraft disposal manoeuvres account for a cumulative Delta V of $\Delta V = 40 \text{ ms}^{-1}$.

A highly elliptical geocentric orbit was considered for this mission. However, the extension of the geocorona, a region rich in neutral hydrogen retained by the Earth's magnetosphere, amounts to roughly 600,000 km in the Sun-Earth direction, pointing away from the Sun. Since neutral hydrogen atoms absorb EUV radiation, it is necessary to make observations outside of the geocorona. Therefore, an obvious location is the Sun-Earth L_2, one of the equilibrium points in the Sun-Earth dynamical system. In particular, the mission will fly in a Halo orbit around the L_2 point. While the in-plane displacement of the orbit is not constrained, the out-of-plane amplitude of the orbit (z-direction) is limited to a maximum value z_{max}. This constraint derives from the required visibility of the New Norcia's ground station at all times during the orbit. The maximum out-of-plane displacement can be computed as follows, which considers the worst-case scenario where the spacecraft is at the maximum positive displacement above the ecliptic during the winter solstice with

$$z_{max} = d \sin \frac{\pi}{2} - \alpha - \theta - \varphi. \tag{1}$$

where α is the minimum elevation angle for communication, θ is the tilt of Earth's axis, φ is the latitude of the ground station, and d is the distance between the Earth and the L_2 point ($d \approx 1.5 \cdot 10^6$ km). With the previous assumptions, a maximum displacement $z_{max} = 645,000$ km can be obtained. The orbital period of the Halo orbit will depend on the in-plane amplitude; however, in order for the orbit to be stable, the period will be constrained to five to seven months. Therefore, the spacecraft will cross the ecliptic plane every three months on average. Since the L_2 point is an unstable equilibrium point, orbit maintenance will have to be performed.

3.2. Ground segment and operations

For the ground segment, the ESA portion of the Deep Space Network was considered given the long distance and high data rates involved, requiring high-performance antennas. Similar to other similar missions, mission control would likely be located at the European Space Operations Centre (ESOC) facilities in Darmstadt, Germany. Mission-critical spacecraft operations data such as telecommands and spacecraft health would be transmitted between the ground station and mission control via the high-speed data links provided by OPSNET (Schulz et al. 2022). Science data can then be distributed to the research community and other interested parties via ESANET, with the European Space Astronomy Centre (ESAC) in Madrid, Spain serving as the main liaison with the science community.

As the mission progresses the spacecraft will transition between different operational modes. The journey from the launch pad to L_2 orbit is expected to last around one month, a period during which the spacecraft will run on a low-power mode, resorting to simple spacecraft health telemetry via the low-gain antennas. The spacecraft features two different scientific observation modes according to the task. In snapshot mode, a single object is observed in the EUV spectrum for approximately ten

hours, whilst in the staring mode, whose main objective is to observe CMEs and flares, a single target is observed for approximately one week.

During programmed communication windows the spacecraft enters a communication mode which prioritises the acquisition of the ground station on Earth. When the signal is acquired, the medium gain antenna activates and begins the downlink of science data.

A safe mode is also provided whereupon the satellite attempts to stabilise itself and orient the solar panels towards the Sun while becoming health data in the low gain antennas in order to assist the ground station in troubleshooting and recovery of the spacecraft. In this mode, all non-essential electronics are turned off to preserve battery power. Moreover, to prevent any damage to the sensors in case of position towards the Sun, the telescope cover is closed.

3.3. Duration and descoping

A mission development schedule of ten years is foreseen to ensure spaceflight readiness of all payload and platform components. This schedule will allow for different testing of both the single elements of the payload module and the Spacecraft (S/C) as a whole. The expected tests to be performed are:

1. Thermal vacuum chamber testing
2. Environmental testing (Helmholtz cage, electromagnetic interference)
3. Vibration and shock tests to ensure the survival of the S/C during the launch phase in Ariane 6.2
4. Detumbling

The nominal lifetime of the mission is five years but two years of mission extensions are taken into account. The disposal of the S/C will take about 6 months.

The main cost drivers of the mission are the mirror and instrument size, the only significant descoping option would be to reduce the mirror size in order to cut down both mass and cost at the expense of S/N and time resolution. The performance of the TT&C could also be descoped to reduce its implementation cost, at the expense of potentially requiring longer communication windows or only collecting a fraction of the science data generated.

3.4. Cost Assessment

A cost breakdown of the different subsystems of the S/C can be seen in Table 1.

Table 1. Risks related to FEAST mission.

Industrial Cost		Million €
	Spacecraft Bus	250
	Payload	150
	Total Industrial Cost	400
ESA Project Cost (25 % of Industrial Cost)		100
Operation		100
	Total	600
	Total with 20 % contingency	720
Launch		90
Total Mission Cost		810

Table 2. Table of costs related to FEAST mission.

3.5. Risk Assessment
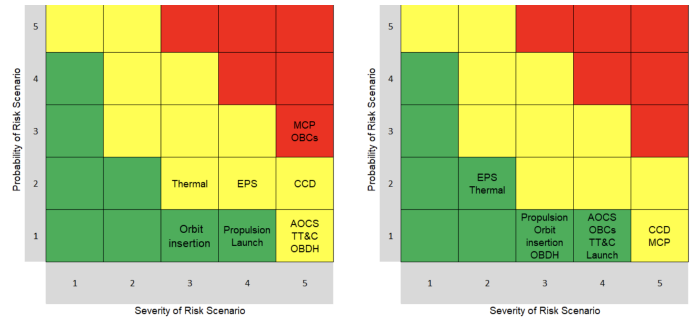
The mission has been designed with components such as the Delta Doped EMCCD that are still in the technology demonstration level (TRL6). These technologies are supposed to mature during the mission development period. During the risk assessment evaluation, ten different risks have been identified spanning from Launcher and Service Module to Payload Module. For all of FEAST's risks proper risk mitigation measures were identified and applied. The main risks are connected to the MCP and the CCDs failures due to an erroneous pointing of the telescope module to the Sun. To prevent such risk a shutter has been included in the Telescope Module and the three Sun sensors present in the S/C should ensure that also during Safe Mode operations the Telescope Module shall never face the Sun directly. The risk for the On-Board Computers was mitigated through additional redundant units and a network topology which allows for a hot backup in case of computer failure, as described in the relevant section. Both the Thermal and EPS systems were likewise mitigated through the implementation of the sun-shield and the existence of redundant units.

4. Payload

The FEAST mission features a spectrograph able to resolve the EUV ($100 - -700$)Å and FUV ($1000 - -1650$)Å spectral ranges. The spectrograph is composed of a grazing incidence modified Hettrick-Boyer Type-1 telescope with an aperture stop in the primary mirror focal plain to achieve a narrow field of view. A transmission diffraction grating in a Rowland torus geometry separates the incident photons by their wavelength deflecting the incident radiation to different spatial locations where multichannel detectors record photon counts. Lastly, the portion of incident photons not deflected by the diffractive element provides a fine guidance system for accurate and stable pointing, allowing us to image the same star over long periods of time.

All of the instrument sizing and requirements[1] are based on the available data from α-Centauri A. recorded by the EUVE and HST/STIS missions [cit needed]. This star was chosen since it has remarkably similar stellar properties to our Sun and is sufficiently far enough so that the attenuation by the ISM plays a signification role allowing us to correctly estimate the amount of EUV photons that reach the close-Earth environment without the need of ISM absorption models.

The first parameter required to design our instrument is the effective area over the required wavelength range, this parameter is computed as the telescope light-collecting area compensated by all of the losses induced by the different components (*e.g* Mirror losses, detectors efficiency,...) The scientific requirements

---

[1] In particular the incident photon flux in the EUV and FUV range.

dictate an observation time of $\Delta t_{obs} = 600$ s to resolve temporally CMEs with a signal-to-noise ratio S/N=100. Given that single photon counting error is dominated by shot noise S/N = $\sqrt{N_{count}}$ the effective area can be computed easily as the area that allows collecting $N_{count} = 10^4$ photons in the observation time. Taking into account typical values of incident photon flux for the dimming and non-dimming lines $\Phi = 1.9 \times 10^{-2}$ photons/s/cm^2 we can estimate an effective area

$$A_e = \frac{10^4}{\Phi \times \Delta t_{obs}} \sim 880 \text{ cm}^2.$$

It is remarkable to mention that this value improves by a factor $\times 100$ the previous results from the EUVE mission which featured $A_e \sim 9$ cm^2. While we argue that shot noise is the major noise source in the signal, a more detailed study is required to assess the significance of noise induced by cosmic rays, this however could be solved using a simple detector in an anti-coincidence configuration to filter out a spoiled result.
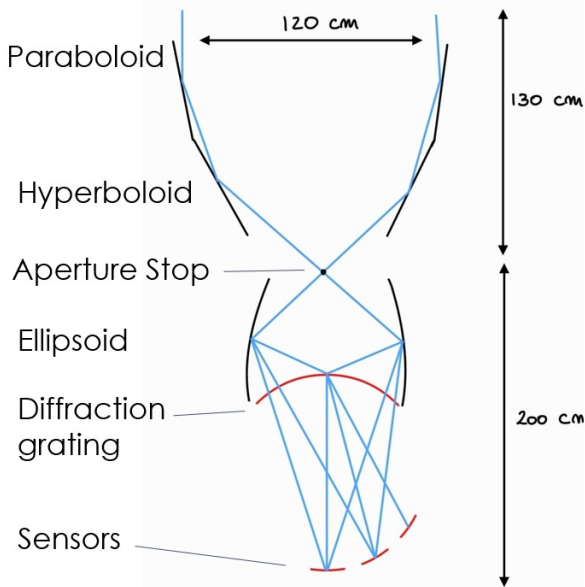
4.1. Optics

Fig. 4.1. Schematic of the main optical component of the FEAST telescope.

The main challenge in designing the optics of a EUV/FUV telescope lies in the grazing angle requirement: as the energy of the incident photon increases the shallower the incidence angle has to be to have a reflection over the mirror surface, in particular for the EUV energy range the grazing angle must satisfy $\theta < 7.9°$ (Hettrick and Bowyer 1984). The configuration adopted is a modified Hettrick-Boyer Type-1: the first stage features multiple nested shells of the parabolic and hyperbolic mirror for a compressive primary focal length of 110 cm, a pinhole of ⌀ 0.5 mm in the focal plane acts as an aperture stop and limits the instrument field of view. Nested elliptical mirrors refocus the converging rays towards the detectors. This configuration differs from the original Hettrick-Boyer I design which only features a parabolic mirror as the primary stage. This modification shortens the primary focus and allows a shorter instrument with an estimated front-to-focus length of 330 cm. [maybe sketch needed?]

The envisioned mirror, made of an Aluminium-Beryllium Alloy with Gold coating should feature a point spread function (PSF) smaller than 1" and a surface roughness smaller than 15 Å. The former requirement is driven by the wavelength resolution (M2, M5) together with the instrument length while the latter condition allows to maintain the coherence of the smallest observed wavelength (150 Å). Given a conservative estimate on the efficiencies for sensors and diffraction element, 40% and 20% respectively we require an aperture of 120 cm.

After the secondary mirror assembly, photons pass through a transmission diffraction grating which separates the incoming photons by their wavelength. For first order diffraction, a given wavelength is deflected by an angle $sin(\alpha) = \lambda/d$ where $1/d$, the line pairs per millimetre, is chosen in a way that allows to separate two resolved wavelengths more than their PSF. In particular the given resolution $\Delta\lambda = 0.2$ Å imposes

$$\Delta\alpha \approx \frac{\Delta\lambda}{d} > \text{PSF} = 1'' \rightarrow 1/d > 250 \text{ mm}^{-1}$$

The chosen value of $1/d$ is 500 mm^{-1} allows us to compute, according to the wavelength range of interest, the position and linear extensions of the detectors. To account for geometry effects a Rowland torus geometry is employed which makes the component more expensive but allows for an overall smaller spacecraft size. This component represents the main loss source in the measuring system: only ~ 20 % of the incident radiation is deflected while roughly ~ 50 % continues along the optical path without being affected.

4.2. EUV detector

Conventional Charge-coupled devices (CCDs) are not sensible in the EUV range, for this reason, we employ a Microchannel plate detector (MCP): the incoming photons set off a shower of electrons which are then captured by an underlying CCD. The chosen model MCP 34-10 (TRL6) is able to cover the required spatial extension of 27.5 mm and features the following technical parameters:

The main downside of this detector is the high voltage required which would require particular attention in handling. For each photon hit the detector microcontroller delivers the pixel position and the clock count for a maximum of 84 bit of data per photon, with the integrated photon flux from α- Centauri. We expect a count rate of 609 photons/s corresponding to 6 kb/s, this should be taken into account when sizing the data buffer.

4.3. FUV detector

Regarding FUV, solid state detectors offer significant advantages over the vacuum tube based technology of MCPs, therefore to surpass the performance of the latter a stable and high QE solid-state detector is needed. NASA's Jet Propulsion Laboratory (JPL) has developed a surface passivation technology known as "Delta Doping". This new kind of EMCCD can achieve high and stable quantum efficiency (around 50 % in FUV). In order to properly function it must be accounted for both Quantum Efficiency Hysteresis (QEH) removal and Quantum Yield (QY) ((Nikzad et al. 2012)).

4.4. Fine guidance system

For accurate and stable pointing we employ the light not deflected by the diffraction element which hits a CCD on the de-

tector plane. We use the same sensor used for the FUV to image the pointed star and continuously compare the projected dot to the equilibrium position. This feedback mechanism allows a nominal precision of 1.15", however, the pointing accuracy and stability will be determined by the speed and precision of the reaction wheels. It is important to notice that this kind of sensor, coupled with a thin band-pass filter in the FUV range, allows to measure the integrated flux adding a layer of redundancy and cross-calibration when compared to the FUV spectrum measured by the FUV detector.
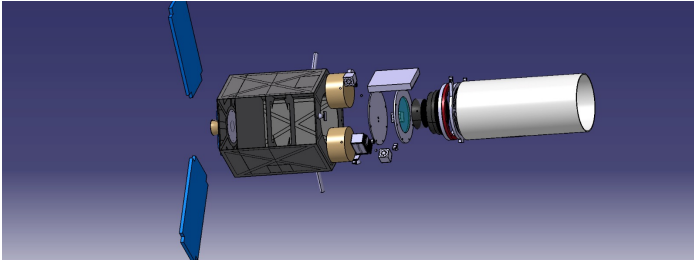
5. Spacecraft

Fig. 5.1. FEAST spacecraft exploded view.

Figure 5 shows the exploded view of the FEAST spacecraft.

5.1. Electric Power System

The Electric Power System (EPS) was designed to provide a minimum of 827 W during nominal science operations and 177 W during survival mode (Launch and Early Operations, Safe Mode). The main drivers for power requirements are the MCP detector (260 W), the heating system for critical components (150 W), the On-Board Computers (100 W), and the losses in DC-DC voltage conversion for the MCP detector. There are also power losses due to the low efficiency of series regulators for the electrical circuit (efficiency as low as 0.3 (Shao et al. 2011)).

To fulfil the power requirements, triple-junction GaAs solar cells have been selected. These have a typical efficiency at Beginning Of Life (BOL) of 26 %, which decreases by 2.5 % each year for several reasons (impact with micrometeoroids, energetic particles, etc...) (Shao et al. 2011). Therefore, the solar panels have been sized based on the End-Of-Life (EOL) efficiency of 13.5 %. The orbit requirements are such that the spacecraft is always out of the penumbra cone reaching the L_2 point; therefore, the maximum power flux from the Sun is always available. Solar Array Driver Assemblies (SADAs) are needed to track the Sun and maximize the efficiency in power harvesting. While two-axis SADAs exist, a single-axis SADA was adopted due to the increased complexity and low flight heritage of two-axis gimbal systems for solar panels. However, using a single-axis SADA imposes a constraint on the angle between the normal to the solar panel and the Spacecraft-Sun direction (δ). The EPS was sized using an angle of $\delta = 60$ to allow the spacecraft to observe a larger portion of the celestial sphere, satisfying the mission requirements. A total area of 7.09 m^2 is sufficient to fulfil the power requirements.

Battery packs are also necessary to ensure the functioning of the spacecraft during Launch and Early Operations (LEOP), but also a minimum lifetime in non-Sun pointing mode during Safe Mode. A primary, non-rechargeable battery pack made of

Lithium Sulfur Dioxide with a capacity of 1000 W/hr was selected to ensure enough power for solar array deployment and early communications with the spacecraft. A secondary battery pack, split into four units for redundancy, was selected to ensure a minimum functioning of the spacecraft for five hours with a power requirement of 177 W. The capacity of each Li-Ion battery unit is 19.75 Wh, while the mass of the entire battery system is 19.13 kg. Lithium-ion batteries require a more stringent operating range with respect to other spacecraft subsystems, therefore patch heaters will be installed around the battery packs.

5.2. Attitude Determination and Control System

High precision pointing accuracy is vital for the scope of the mission and for successful readings from the sophisticated telescope unit. For a more coarse pointing adjustment two 3-axis MEMS gyros (one for redundancy) are mounted on the spacecraft. Moreover, two Star Trackers (one for redundancy) are mounted aligned to the telescope unit in order to achieve a pointing accuracy of 30".

Despite the star trackers and gyros, the sensors mounted up to now, while ensuring a fine pointing of the telescope unit, still don't guarantee a 1:1 correspondence between what the telescope is pointed at and what the detectors are observing. This is due to the fact that there is some angular shift between the star trackers and the detectors inside the telescope unit. A Fine Guidance Sensor (an EMCCD) is therefore mounted inside the telescope unit to ensure that the detectors are observing the desired target with a 1.6" accuracy.

Three Sun sensors are then orthogonally mounted – one per axis – in order to prevent the telescope unit from pointing at the Sun during Safe Mode operations.

Four reaction wheels are mounted in a 123 configuration (one for redundancy) which ensures a minimum slew angle of 33'. Four more smaller reaction wheels are then mounted to ensure finer adjustment movements of the S/C in order to comply with the FGS requests.

5.3. Propulsion

A chemical (hydrazine) propulsion system has been chosen to comply with our scientific requirements for mission duration. Hydrazine thrusters are used to perform manoeuvres to correct for the launcher's inaccuracy, orbit insertion, orbit maintenance (once every six months), periodic wheel offloading, as well as end-of-life disposal. One primary nozzle and eleven identical secondary nozzles (for redundancy) were selected. The primary nozzle is used for orbit insertion, maintenance, and end-of-life manoeuvres; the secondary nozzles are mainly used for wheel offloading and are therefore positioned on different sides of the spacecraft. The specific impulse of the selected hydrazine thrusters is $I_{sp} = 218$ s. The hydrazine is stored in two identical Titanium tanks ($\approx$59 litres each, one for redundancy), located next to the primary nozzle. The cumulative mass of the tanks amounts to approximately 19 kg. The total mass of propellant to ensure a nominal mission duration of five years is 117 kg. The total mass of the propulsion system is estimated to be around 267 kg. The calculated Δv budget is shown in table 5.3.

5.4. On-Board Computer

Our interface has eight onboard computers (OBC) which are in charge of the data handling in the system. They are connected

Table 3. Calculated Δv budget for the mission.

Operation	Orbit Δv (m/s)
Initial L_2 orbit injection	40
Orbit Station-Keeping (per year)	6
Orbit Station-Keeping (required)	24
Orbit Station-Keeping (goal)	36
Graveyard Orbit Injection	30
Total	136
Total +100% margin	272

in pairs to the detectors for redundancy and therefore risk mitigation. Moreover, each subsystem is connected to each OBC in a mesh network topology to assure better redundancy and risk mitigation, at the expense of a marginal increase in cost and network complexity. The processor architecture used is the LEON-FT, a general-purpose space-qualified microprocessor developed by ESA and employed in similar missions such as Euclid for its OBC system (Racca et al. 2016).

Using the On-Board Data Handling Subsystem (OBDHS) all data received from the detectors goes through a buffer and then reaches cold memory. Prolonged operations are guaranteed thanks to the flushing of the buffer every 60 s. Based on payload instrument data generation rates, a buffer size of at least 17 MB is necessary for each of the three instruments. Since the Staring spacecraft operation mode is capable of requiring up to one week of uninterrupted data gathering, it may be necessary to store at least as much time worth of science data. In addition to this, the cold memory storage was sized to also store up to one month of spacecraft telecommand and health data to facilitate troubleshooting and diagnosis for spacecraft operators. For these reasons, cold memory storage of at least 30 GB is required. During the downlink window, the data goes from the cold memory to Earth's ground station after implementing data compression algorithms.

5.5. Telemetry, Tracking & Control system

The Telemetry, Tracking Control system (TT&C) allows for the monitoring and remote operation of the spacecraft platform and payload instrumentation as well as for the relay of science data.

The full capability of the ESTRACK and Deep Space networks can easily provide round-the-clock communications coverage to a spacecraft located in L_2, however, leasing more ground stations for longer periods of time results in larger operational costs and (especially in the case of the Deep Space antennas) constrain the operational capability of ESA for other missions. The ESTRACK ground station in New Norcia, Australia was considered as the only ground station for the FEAST mission, with its 35 m diameter deep space NNO-1 antenna in the X-band as the primary communications antenna. Assuming that the L_2 orbit constraints regarding out-of-plane offsets are satisfied and that the ground station antenna can gimbal and track the satellite from elevation angles above $10°$, an effective field of view of approximately $160°$ is established from the ground station, resulting in a potential coverage availability of about 10.6 hours every day. Of these, 2 hours of communication window is proposed where the spacecraft is expected to offload up to a week of science data to account for extended science gathering sessions or in case of safe modes or missed communication windows.

The spacecraft is designed to have a medium gain array (MGA) for primary data downlink. A single parabolic cassegrain

X-band antenna architecture was chosen for a high transmitting and receiving gain, at the expense of being directional and requiring the spacecraft to have a communications mode where it must orient the antenna towards the ground station, thus interrupting scientific data collection. A fixed antenna was selected to reduce cost, manufacturing complexity, power consumption and additional points of failure. A low gain array (LGA) was included to confer the spacecraft with a baseline communications capability regardless of its orientation in the case of priority telecommands, safe mode or tumbling. For this purpose two S-band omnidirectional antennas were selected and sized based on existing technology such as those used in the NASA International Cometary Explorer spacecraft (Hilliard 1987), with each offering at least $180°$ coverage and placed on opposite sides of the spacecraft, also offering a degree of redundancy.

Table 4. Breakdown of the Uplink and Downlink data rates.

Uplink (kb/s)		Downlink (Mb/s)	
Telecommand	24	S/C Health	0.02
		Payload	0.01
		Science Data	168.21
Total	24		168.24

With the prescribed communication windows and payload instrument data generation rates, a breakdown of the uplink and downlink data rates was produced, shown in Table 4. The X-band and S-band comprise a range of known frequencies, which are defined alongside the turnaround ratio by the Consultative Committee for Space Data Systems (Synchronization 2012). The sizing of the MGA and LGA was carried out using the link budget equation, expressed in decibel format as

$$SNR = P + L_l + G_t + L_s + L_a + G_r + 228.6 - 10\log T_s - 10\log R \quad (2)$$

where the first three terms refer to the transmitter, L_s and L_a being functions of the signal path (constrained by the L_2 orbit) and RF frequency selection, the following three terms being functions of the receiver and R being the data rate (Shao et al. 2011). The calculations were performed in both uplink and downlink situations, with the MGA sized for nominal operation and the LGA sized for data rates expected during safe mode (only downlink of spacecraft and instrument health data). A variety of parabolic Cassegrain antennas were researched to obtain a trend between antenna diameters and their respective masses, allowing for a rough estimation of the parabolic antenna mass. Based on these calculations, the MGA antenna has a minimum receiver gain of -35.0 dB (essentially it is not a significant constraint), a minimum diameter of 76 cm with a mass of 8.56 kg. On downlink at least 100 W of power are required and the transceiver gain must be at least 33.8 dB, with a beam width angle of $15.6°$. Although the LGA antenna was already predefined based on existing technology, the link budget was used to verify the component's adequacy (minimum receiver gain of -20.0 dB and minimum transmitter gain of 6.7 dB are required, and the antenna has a gain of at least 7dB in the $180°$ beam range) and to verify that power consumption of 10 W can be achieved (Hilliard 1987).

The remaining TT&C hardware such as the Central Data Management Unit is selected to be of conventional spacecraft architecture and similar to missions such as Gaia and Euclid and featuring hot dual-redundancy to increase the reliability of the hardware and data flow system. As the spacecraft features RF

communications capabilities in the X- and S- bands, it is compatible with other ground stations in the broader ESTRACK network. In the event of failure of the MGA, it is possible to use the LGAs for a limited science data downlink of approximately 25 kb/s, preserving mission integrity in exchange for a more constrained science output.

5.6. Thermal System

The thermal equilibrium of the spacecraft, assuming that the spacecraft radiates like a black body at a uniform temperature of T_{SC}, is the following:

$$S_{in}Q_{in}\alpha = S_{out}\epsilon\sigma T_{SC}^4 \tag{3}$$

where S_{in} and S_{out} are respectively the absorbing and emitting surface areas, α and ϵ are respectively the absorption and emission coefficients, and σ is the Stephan-Boltzmann constant (Shao et al. 2011); finally, Q_{in} is the radiative flux at the L_2 point. The environment around the L_2 point is thermally stable, as the main thermal load is the Sun's radiative flux, equal to $Q = 1339\,\mathrm{W m^{-2}}$ (Shao et al. 2011). A secondary source of thermal load is the heat produced by electronics, which was estimated to be around $Q_{elec} = 200$ W. All other sources of heat are negligible. Most subsystems of the spacecraft have an allowed operating range of [-20, +50] °C that can be reached with Multi-Layer Insulation materials, such as Aluminized Kapton, enabling an absorptivity coefficient of $\alpha = 0.35$ and an emissivity coefficient of $\epsilon = 0.85$ (Shao et al. 2011). However, to maintain this temperature range, constraints on the minimum and maximum angle $\beta = \hat{\mathbf{Z}}\hat{\mathbf{x}}$ between the spacecraft's X-axis and the ecliptic would arise This is because the effective absorption area of the space varies as follows:

$$S_{in} = \frac{1}{2}S_{SC}\beta \tag{4}$$

where S_{SC} is the total external area of the spacecraft. At high values of this angle, the absorption area increases, driving the equilibrium temperature outside of the requirements. Therefore, a maximum angle β_{max} should be imposed on the attitude of the spacecraft. This configuration would impose hard constraints on the observable portions of the celestial sphere. In addition, the thermal expansion of the telescope's optical components should be kept below the required threshold (FE-SCI-010, FE-SCI-051). This is not possible with MLI. Therefore, two alternative solutions have been designed:

1. A large deployable shield beneath the payload module with optimal thermoelastic behaviour. Made of multi-layer insulation sheets, it is attached to the service module and folded against the payload module.
2. A Sun Shield part of the service module that consists of a carbon fibre reinforced plastic (CFRP) frame made of two vertical poles with diagonal stiffeners and two struts slanting toward the service module.

The most important downsides of the first concept are the significant mass increase and the increased complexity needed for the deployment. On the other hand, the other concept would greatly reduce the number of observable stars, as it would impose a constraint on the minimum angle β_{min}. Therefore, the first solution must be employed to comply with science requirements (FE-SCI-010, FE-SCI-051). Such a sun-shield would ensure an absorption coefficient as low as $\alpha = 0.05$, resulting in operating temperature ranges of [-87.63, -54.35] °C. While this solution

ensures sufficiently low levels of thermal noise and thermal expansion for the optics, it will require extensive testing for the deployment system due to the relatively low maturity level of the technology. The experience acquired on the Gaia sun-shield will be helpful in the design and development of the FEAST sun-shield.

The sun-shield will have a radius of $R_{ss} = 0.9\,h_{SC}$, where h_{SC} is the length of the spacecraft. Therefore, the spacecraft will be able to continuously observe the celestial sphere with a maximum angle $|\beta_{max}| = 45°$. Thanks to the addition of MLI around the telescope, this angle can be increased to $|\beta_{max}| = 55°$ for a limited amount of time (roughly ten hours), which allows observing an increased number of stars in survey mode.

Active thermal control devices will be required for different reasons. Patch heaters will be needed to maintain batteries and hydrazine tanks at an operating temperature $T_{min} > 10°C$. The MCP detector also needs to be heated to an operating temperature of $T_{min} > 0°C$; given the small size of the detector, a cartridge heater will likely suffice. Furthermore, electronic components producing heat will be insulated from the rest of the spacecraft through MLI and dedicated radiators will dissipate the heat in excess.

5.7. Structure

The telescope payload requires high positioning accuracy and high dimensional stability in order to achieve the required optical performances. A rigid structure must therefore be designed to support the telescope ensemble with minimal thermal warping (complementing the Sun Shield) while also resisting transient loads from the launch environment.

To this extent the majority of the spacecraft structure is made out of Silicon Carbide ceramic, which not only boasts a low thermal expansion coefficient of but also a high thermal conductivity, minimizing overall thermal expansion of the structure as well as reducing anisotropic structural warping due to thermal gradients across the spacecraft. This material also has a large elastic modulus relative to its density, enabling the structure to be relatively lightweight and reducing the overall mass of the spacecraft.

5.8. Budgets

Design budgets were elaborated to describe the mass breakdown of the spacecraft, a power consumption across the different spacecraft systems. Uncertainty margins were implemented depending on low TRL or projected information (Shao et al. 2011). The Δv budget has already been discussed and can be seen in Table 5.3.

The mass and power budget breakdowns are reported respectively in Table 5 and Table 6.

5.9. Mission Schedule and Descoping options

A mission development schedule of ten years is foreseen to ensure spaceflight readiness of all payload and platform components. This schedule will allow for different testing of both the single elements of the payload module and the S/C as a whole. The expected tests to be performed are:

1. TVAC Test
2. Environmental testing (Helmholtz cage, EMI)
3. Vibration/Shock tests to ensure the survival of the S/C during the launch phase in Ariane 6.2
4. Detumbling

Table 5. Mass budget of the FEAST mission. M_{mar} indicates the mass with margin (usually 20%), while M_{dry} is the dry mass of the spacecraft.

Module	System	M [kg]	M_{mar} [kg]	% of M_{dry}
Payload	Telescope	350	420	27 %
Service	Propulsion	105	150	10 %
	Power	110	165	11 %
	Thermal	140	168	11 %
	TT&C	40	48	3 %
	Structure	405	486	31 %
	ADCS	35	71	4 %
	OBC	40	48	3 %
	Total	875	1137	68 %
Dry mass			1557	100 %
Wet mass			1674	107 %

Table 6. Power budget of the FEAST mission.

	Nominal Power (W)	Safe Model (W)
Payload Module		
MCP	260	0
EMCCD	0.1	0
CCD	0.1	0
Payload Total	260	0
Service Module		
Heater	150	38
TT&C	10	10
Propulsion	0	30
OBCs	100	25
ADCs	55	64
EPS	125	13
Service Total	495	262
Grand Total +20 %	906	314

The nominal lifetime of the mission is five years but two years of mission extensions are taken into account. The disposal of the S/C will take six months.

The main cost and mass driver of the mission are the mirror and instrument size, the only significant descoping option will be to reduce the mirror size in order to cut down both mass and cost at the expense of S/N and time resolution. The performance of the TT&C could also be descoped to reduce its implementation cost, at the expense of potentially requiring longer communication windows or only collecting a fraction of the science data generated.

5.10. Public outreach

The outreach plan aims to showcase the mission to a broad audience and to increase public awareness and interest in both the mission and the broader field of astrophysics and plasma physics. This would be achieved through advertisement across all social media platforms and collaboration with academic and research institutions. In particular, the outreach activities should be actively geared towards groups underrepresented in science and astrophysics, for example by participating in programs targeting schools in disadvantaged areas and using data collected by FEAST to inspire and educate young people there.

6. Conclusion

The FEAST mission will further our understanding of the formation of high-energy events in Sun-like stars and the influence of the EUV radiation on exoplanets' atmospheres. The unique optical design will for the first time allow to probe of the corona of nearby Sun-like stars and link CMEs and flares to stellar properties, in addition, it will allow studying the influence of the EUV radiation on the upper atmosphere of the exoplanets in those systems. The spacecraft platform consists of a telescope assembly with detectors for the EUV and FUV range. The telescope uses a modified Hettrick-Boyer type 1 optical assembly. In order to maximise efficiency, spectral resolution and Signal-to-noise ratio, the telescope will be stationed at L_2. This is achievable with our spacecraft and its bespoke electronics with an important heritage from past missions such as SOHO, Chandra and HST.
This mission will bridge the existing gap in our knowledge on the habitability of exoplanets based on their nearby stellar activity.

References

Bowyer, S. (1991). The euve missions. *Bulletin of the American Astronomical Society*, 23:972.

Cecchi-Pestellini, C., Ciaravella, A., Micela, G., and Penz, T. (2009). The relative role of EUV radiation and X-rays in the heating of hydrogen-rich exoplanet atmospheres. *Astronomy & Astrophysics*, 496(3):863–868.

Cheng, J. and Qiu, J. (2016). The nature of cme-flare-associated coronal dimming. *The Astrophysical Journal*, 825(1):37.

France, K., Fleming, B., Youngblood, A., Mason, J., Drake, J. J., Amerstorfer, U. V., Barstow, M., Bourrier, V., Champey, P., Fossati, L., et al. (2022). Extreme-ultraviolet stellar characterization for atmospheric physics and evolution mission: motivation and overview. *Journal of Astronomical Telescopes, Instruments, and Systems*, 8(1):014006.

Ganguli, S. B. (1996). The polar wind. *Reviews of Geophysics*, 34(3):311–348.

Hettrick, M. C. and Bowyer, S. (1984). Grazing incidence telescopes: a new class for soft x-ray and euv spectroscopy. *Applied optics*, 23(21):3732–3735.

Hilliard, L. M. (1987). Performance characteristics of omnidirectional antennas for spacecraft using nasa networks. Technical report.

Lagier, R. et al. (2021). Ariane 6. *User's Manual*, (1).

Lammer, H., Selsis, F., Ribas, I., Guinan, E., Bauer, S., and Weiss, W. (2003). Atmospheric loss of exoplanets resulting from stellar x-ray and extreme-ultraviolet heating. *Astrophysical Journal - ASTROPHYS J*, 598.

Lehner, N., Jenkins, E., Gry, C., Moos, H., Chayer, P., and Lacour, S. (2003). Far ultraviolet spectroscopic explorer survey of the local interstellar medium within 200 parsecs. *The Astrophysical Journal*, 595(2):858.

Mason, O., Scott, N., González, A., Robbins-Pianka, A., Baelum, J., Kimbrel, J., Bouskill, N., Prestat, E., Borglin, S., Joyner, D., Fortney, J., Jurelevicius, D., Stringfellow, W., Alvarez-Cohen, L., Hazen, T., Knight, R., Jack, G., and Jansson, J. (2014). Mason et al., 2014.

Moschou, S.-P., Drake, J. J., Cohen, O., Alvarado-Gómez, J. D., Garraffo, C., and Fraschetti, F. (2019). The Stellar CME–Flare Relation: What Do Historic Observations Reveal? *The Astrophysical Journal*, 877(2):105.

Nikzad, S., Hoenk, M. E., Greer, F., Jacquot, B., Monacos, S., Jones, T. J., Blacksberg, J., Hamden, E., Schiminovich, D., Martin, C., and Morrissey, P. (2012). Delta-doped electron-multiplied ccd with absolute quantum efficiency over 50applications. *Applied Optics*, 51:365–369.

Racca, G. D., Laureijs, R., Stagnaro, L., Salvignol, J.-C., Alvarez, J. L., Criado, G. S., Venancio, L. G., Short, A., Strada, P., Bönke, T., et al. (2016). The euclid mission design. In *Space telescopes and instrumentation 2016: optical, infrared, and millimeter wave*, volume 9904, pages 235–257. SPIE.

Rumph, T., Bowyer, S., and Vennes, S. (1994). Interstellar medium continuum, autoionization, and line absorption in the extreme ultraviolet. *The Astronomical Journal*, 107:2108–2114.

Schulz, K.-J., Christ, U., and Fay, J. (2022). Esa's operational network for future missions -the introduction of internet technologies.

Shao, A., Maruyama, C., and Greer, J. (2011). *Space mission engineering - the new SMAD*. *Workbook*. Hawthorne, Ca Microcosm Press.

Synchronization, T. (2012). Channel coding—summary of concept and rationale. *Report Concerning Space Data System Standard. Informational Report CCSDS*.

Veronig, A. M., Gömöry, P., Dissauer, K., Temmer, M., and Vanninathan, K. (2019). Spectroscopy and differential emission measure diagnostics of a coronal dimming associated with a fast halo cme. *The Astrophysical Journal*, 879(2):85.